AD-A133 430 SHORT-RANGE ACOUSTIC INTENSITY VECTORS OF THE PEKERIS SHALLOW WATER MODEL..(U) ADMIRALTY MARINE TECHNOLOGY ESTABLISHMENT TEDDINGTON (ENGLAND.. E A SKELTON AUG 83 1/1

UNCLASSIFIED AMTE(N)/TM83065 DRIC-BR-88937 F/G 20/1 NL

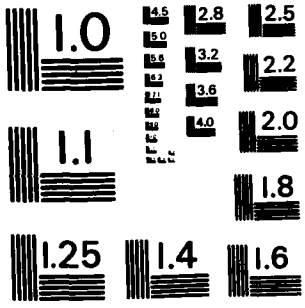

MICROCOPY RESOLUTION TEST CHART
NATIONAL BUREAU OF STANDARDS-1963-A

AMTE(N)TM83065

SHORT-RANGE ACOUSTIC INTENSITY VECTORS OF THE PEKERIS SHALLOW WATER MODEL

BY

E.A. SKELTON

Summary

Intensity vectors of the Pekeris model are calculated from values of acoustic pressure and particle velocity which are obtained by numerical integration. Plots of the vectors, for the cases of no-seabed, a rigid seabed and fast and slow seabeds, illustrate the potential usefulness of the intensity vector approach as an aid to understanding the physics of underwater sound propagation.

AMTE(Teddington)
Queen's Road
TEDDINGTON Middlesex TW11 0LN

34 pages
13 figures

August 1983

CONTENTS

LIST OF SYMBOLS

(r,z)	cylindrical coordinates
$p_1(r,z)$, $p_1^*(r,z)$	acoustic pressure in the layer and its complex conjugate
$p_2(r,z)$, $p_2^*(r,z)$	acoustic pressure in the half-space and its complex conjugate
$V_{1r}(r,z)$, $V_{1z}(r,z)$	radial and axial particle velocities in the layer
$V_{2r}(r,z)$, $V_{2z}(r,z)$	radial and axial particle velocities in the half-space
$I_{1r}(r,z)$, $I_{1z}(r,z)$	radial and axial acoustic intensities in layer
$I_{2r}(r,z)$, $I_{2z}(r,z)$	radial and axial acoustic intensities in half-space
$I_1(r,z)$, $\Theta_1(r,z)$	amplitude and phase of intensity in the layer
$I_2(r,z)$, $\Theta_2(r,z)$	amplitude and phase of the intensity in half-space
ω	radian frequency ($=2\pi f$)
ρ_1, c_1	density and sound speed in the layer
ρ_2, c_2	density and sound speed in the half-space
k_1, k_2	acoustic wavenumbers, $k_i = \omega/c_i$, i=1,2
b	$= \rho_1/\rho_2$
H	depth of the water
P_0	amplitude of the point source
z_0	distance of the point source above seabed
α	radial wavenumber
α_n	$=[k_1^2-(2n+1)^2\pi^2/4H^2]$, n=0,1,2,...
β_1,β_2	vertical wavenumbers, $\beta_i = [k_i^2-\alpha^2]^{1/2}$, $\mathrm{Im}[\beta_i] \geq 0$, i=1,2
η_1,η_2	hysteretic loss factors
$D(\alpha,\omega)$	dispersion relation, $D(\alpha,\omega) = \beta_1\cos(\beta_1 H)-ib\beta_2\sin(\beta_1 H)$
$R(\Theta)$	plane-wave reflection coefficient
δ	Dirac delta function
$J_0(x)$, $J_1(x)$	Bessel functions of orders 0 and 1
$H_0(x)$, $H_1(x)$	Hankel functions of orders 0 and 1. $H_n=J_n+iY_n$.

INTRODUCTION

Sound propagation in the sea can be a complex process for which mathematical models of varying complexity have been developed. The Pekeris model is the most basic of these; it consists of a homogeneous layer of fluid, which contains a time-harmonic point source of sound, lying over an infinite half-space of another homogeneous fluid [1-3]. Numerical values of pressure obtained from this model are usually presented as plots of propagation-loss versus range, at a fixed depth; or alternatively, as a contour plot of transmission loss over depth and range. Jensen & Kuperman [4] use both these presentations in their report which compares numerical results which were obtained from various theoretical propagation models, which are also described. Little progress has been reported in the presentation of experimental measurements since Wood's scale model work [5].

Plots of acoustic intensity vectors show not only the magnitude of the energy flow but also its direction. Hence, intensity vector plots enable an analyst to distinguish between cases in which there is a net outflow of energy, and those cases in which the energy circulates in closed loops. Pettersen [6] has presented plots which show energy flowing from some simple source and sink configurations, and also plots which show diffraction around and reflection from a thin barrier. Spicer [7] and James [8] have computed acoustic intensity vectors, for a fluid-loaded plate and shell, respectively, which help to illustrate the physics of fluid-structure interaction. Publications by Fahy [9] and Reinhart & Crocker [10] have demonstrated that the 'two-microphone technique' is now a practical tool for the experimental measurement of acoustic intensity.

In this memorandum, the mathematical formulae needed to evaluate numerically the pressure and velocity fields, of the Pekeris model, are given for the special cases of no-seabed, a rigid-seabed, and fast and slow seabeds. The calculation of intensities from numerical values of acoustic pressure and particle velocity is straightforward. Plots of intensity vectors at low frequencies and over short-ranges are presented and discussed. These intensity vector plots reinforce previous numerical work on the Pekeris model, and it is hoped that they will prove to be of sufficient interest to encourage similar presentations in work on more realistic models. The mathematics necessary to extend the work contained here to the model consisting of an arbitrary number of homogeneous layers of fluids and elastic solids is described elsewhere [11,12]. In the more realistic models a rich spectrum of propagating waves, such as the Stoneley and Rayleigh interface waves, may be excited and it is expected that intensity vector plots may reveal which of these propagating waves are likely to be detected experimentally.

2. PROBLEM FORMULATION

The Pekeris model for sound propagation in a shallow ocean consists of a time-harmonic point source of sound, of free-field pressure $p_0 \exp(ik_1 R_0 - i\omega t)/R_0$, which is located in a layer of homogeneous acoustic fluid, whose upper boundary $z=H$ is in contact with a vacuum, and whose lower boundary $z=0$ is in contact with a half-space of a second homogeneous acoustic fluid. This geometry is shown in Figure 1.

The differential equations satisfied by the acoustic pressure, expressed in cylindrical polar coordinates and omitting the time variation $\exp(-i\omega t)$, for this axisymmetric problem are

$$\nabla^2 p_1(r,z) + k_1^2 p_1(r,z) = -4\pi\delta(r)\delta(z-z_0)/r \qquad (2.1)$$

$$\nabla^2 p_2(r,z) + k_2^2 p_2(r,z) = 0 \qquad (2.2)$$

The boundary conditions of continuity of pressure at the boundaries of the fluid layer are

$$p_1(r,H) = 0 \qquad (2.3)$$

$$p_1(r,0) = p_2(r,0) \qquad (2.4)$$

and continuity of normal displacement at the interface between the fluid layer and the fluid half-space requires that

$$(1/\rho_1)[\partial p_1(r,z)/\partial z]_{z=0} = (1/\rho_2)[\partial p_2(r,z)/\partial z]_{z=0} \qquad (2.5)$$

The remaining boundary conditions are those imposed by the radiation condition, viz., at large distances from the source the pressure consists only of outgoing waves. The solutions of equations (2.1) - (2.5) are well known and are summarised in the Appendix for special cases of the seabed constants.

The time-averaged acoustic intensity vectors in the fluid layer have radial and vertical components defined by

$$I_{1r}(r,z) = (1/2)\,\mathrm{Re}[p_1^*(r,z)V_{1r}(r,z)] \qquad (2.6)$$

$$I_{1z}(r,z) = (1/2)\,\mathrm{Re}[p_1^*(r,z)V_{1z}(r,z)] \qquad (2.7)$$

The amplitude and phase of the vectors are

$$I_1(r,z) = [I_{1r}^2(r,z) + I_{1z}^2(r,z)]^{1/2} \tag{2.8}$$

$$\Theta_1(r,z) = \tan^{-1}[I_{1z}(r,z)/I_{1r}(r,z)] \tag{2.9}$$

Equations (2.6) - (2.9) also apply to the fluid half-space if the subscript 1 is replaced by the subscript 2.

3. NUMERICAL RESULTS

(a) General

Fortran computer programs have been written to calculate and store on a disk file the numerical values of pressure and particle velocities at points on a selected grid in the r-z plane, for the various types of seabed considered here. A separate Fortran program uses this data to form and plot the time-averaged intensity vectors.

The numerical constants in SI units used to produce the results shown in Figures 2-13 are:

Fluid Layer	ρ_1 =1000.0	c_1 =1500.0	H=80.0	z_0 =55.0
Fast Fluid Seabed	ρ_2 =1500.0	c_2 =1650.0		
Slow Fluid Seabed	ρ_2 =1500.0	c_2 =1350.0		

The integrals in equations (A7-A15) must be evaluated numerically because closed form expressions are not available. Because the Hankel transform representation is arbitrary with respect to a solution of the homogeneous wave equation, it is necessary to introduce damping into the system in order to lift the poles off the real-axis. Damping is included by setting the sound speeds in the fluids to the complex values

$$\begin{aligned} c_1 &= c_1(1-i\eta_1) \\ c_2 &= c_2(1-i\eta_2) \end{aligned} \tag{3.1}$$

where η_1 and η_2 are chosen as 0.001. This value is sufficiently small

to avoid significant attenuation in the fluids over the distances considered, yet it is large enough to allow numerical integration without ill-conditioning being present. The numerical approximation of the integrals, after truncating the infinite limit to a sufficiently high value, is accomplished by a simple adaptive Gaussian quadrature scheme. Parallel computation on an array of r-values results in a considerable saving in computer time.

In Figures 4-13 the plotted lengths of the normalised vectors are proportional to $R_{QV}(I)$, which is a spherical spreading correction.

(b) Radial Wavenumber-frequency Plots

The dispersion relation for free-waves propagating in the dissipation-free system is obtained from the denominator of the integrands as

$$D(\alpha,\omega) = \beta_1 \cos(\beta_1 H) - ib\beta_2 \sin(\beta_1 H) = 0 \qquad (3.2)$$

The real values of α which satisfy this equation are the radial wavenumbers at which free-waves propagate. The complex values of α represent evanescent waves which decay rapidly with increasing radial distance from the source. The solution $\alpha=k_1$ is trivial.

In the absence of a seabed there are no free-waves of finite wavenumber, and the special case of a rigid seabed gives free-waves whose cut-on frequencies are

$$f_n = (2n+1)c_1/4H \quad , \quad n=0,1,2,... \qquad (3.3)$$

and whose real wavenumbers are given by

$$\alpha_n = (2\pi/c_1)(f^2-f_n^2)^{1/2}, \quad n=0,1,2,... \qquad (3.4)$$

A slow seabed $c_2<c_1$ has no free-waves. A fast seabed $c_2>c_1$ has free-waves whose cut-on frequencies are

$$f_n = (2n+1)c_1c_2/4H(c_2^2-c_1^2)^{1/2}, \quad n=0,1,2,... \qquad (3.5)$$

and whose real wavenumbers are constrained to lie inside the interval

$$k_1 > \alpha > k_2$$

Figure 2(a) shows the wavenumber-frequency plot of the rigid seabed where free-waves cut-on at frequencies 4.7Hz, 14.1Hz and 23.4Hz. Figure 2(b) shows the wavenumber-frequency plot of the fast seabed, where a single branch cuts-on at 11.3Hz. The lines $\alpha=k_1$ and $\alpha=k_2$, between which the real wavenumbers for the fast seabed are constrained to lie, are included on the plot as reference lines.

(c) The Reflection Coefficient

The plane-wave reflection coefficient at the seabed

$$R(\theta) = [\rho_2 c_2 \cos\theta - \rho_1 \sqrt{(c_1^2 - c_2^2 \sin^2\theta)}]/[\rho_2 c_2 \cos\theta + \rho_1 \sqrt{(c_1^2 - c_2^2 \sin^2\theta)}] \qquad (3.6)$$

is of interest because the transform representation of the pressure field resolves the pressure in the fluid layer into a continuous spectrum of waves propagating both upwards and downwards at angles of incidence θ given by the equation

$$\alpha = k_1 \sin\theta$$

In Figure 3(a) the magnitude of the reflection coefficient for the slow seabed decreases steadily with increasing θ until it vanishes at the angle of perfect transmission, $\theta=64°$. At larger values of θ the magnitude of the reflection coefficient increases steadily, attaining its maximum value of unity at $\theta=90°$.

In Figure 3(b) the magnitude of the reflection coefficient for the fast seabed is an almost constant 0.25 until $\theta=40°$. It then increases rapidly to the value of unity at $\theta=65°$, the case of perfect reflection, after which it remains at unity.

(d) Intensity Vector Plots at 2.5Hz

Figures 4 and 5 show the intensity vector plots at a frequency of 2.5Hz where the wavenumber-frequency plots of Figure 2 show that there are no propagating modes. There is little difference between the plots for no seabed, the slow seabed and the fast seabed, all of which show the characteristics of a dipole sound source [6] where most of the sound energy is transmitted into the seabed. The case of the rigid seabed is somewhat special because the intensity is only non-zero by virtue of the finite value of η_1. Here the energy, which is two orders of magnitude smaller than that of the other plots, is being absorbed in the layer.

(e) Intensity Vector Plots at 5.0Hz

Figures 6 and 7 show the intensity vector plots at a frequency of 5.0Hz, where the wavenumber-frequency plots of Figure 2 show that a propagating mode is present only in the rigid seabed case. This mode quickly becomes dominant as r increases, its intensity vector components being

$$I_r \sim \cos^2(\pi z/2H)/r, \quad I_z = 0$$

Again, there is little difference between the plots for no seabed, the slow seabed and the fast seabed, where the intensity vectors exhibit the characteristics of dipole radiation of energy into the seabed.

(f) Intensity Vector Plots at 15.0Hz

Figures 8 and 9 show the intensity vector plots at a frequency of 15.0Hz, where the wavenumber-frequency plots of Figure 2 show that two propagating modes are present in the rigid seabed case, and one is present in the fast seabed case. Again the plots for no seabed and the slow seabed approximate to dipole radiation of energy into the seabed.

In Figure 8(b) the two propagating modes combine to produce an interference pattern which shows energy propagating along the layer with non-zero vertical intensity vector components although the intensity vectors of the separate modes are everywhere horizontal. This is because intensities do not add linearly - the pressure of the first mode interacts with the velocity of the second mode and vice versa, Schultz [13]. The total energy flow is, however, the sum of the energies contained in the individual modes because the contribution of the cross-terms, when integrated across the layer thickness, is zero.

In Figure 9(b), at small distances from the source the intensity vectors approximate to those of dipole radiation of energy into the seabed. At larger distances the propagating mode, whose cut-on frequency is 11.3Hz, interacts with an evanescent mode to produce a closed loop of energy circulation. The propagating mode may be resolved into two waves, one of which propagates upward and the other downward, their angle of incidence being greater than the 65° at which perfect reflection occurs. This mode just begins to dominate at the maximum range shown, viz. 150m.

(g) Intensity Vector Plots at 25.0Hz

Figures 10 and 11 show the intensity vector plots at a frequency of 25.0Hz where the wavenumber-frequency plots of Figure 2 show that three propagating modes are present in the rigid seabed case and one is present in the fast seabed case. The plots for no seabed and the slow seabed are similar and are typical of intensity patterns obtained from well-separated sources.

In Figure 10(b) the three propagating modes combine to produce an interference pattern which shows energy propagating horizontally at the top and bottom of the layer. The plot for the fast seabed, Figure 11(b), is not unlike the plots of Figure 10(a) and 11(a); the single propagating mode does not dominate the solution until radial distances are in excess of 300m (not shown).

(h) Intensity Vector Plots in the Seabed

Figures 12 and 13 show the intensity vector plots, at a frequency of 25.0Hz, in the slow and fast seabeds respectively. The reduction in magnitude of the vectors as the interface is crossed is presumably due to partial reflection at the seabed. As predicted by Snell's law, the intensity vectors in the slow seabed are refracted slightly towards the normal, while the intensity vectors in the fast seabed are refracted away from the normal.

4. CONCLUDING REMARKS

Formulae have been given from which values of the acoustic intensity vectors of the Pekeris model of underwater sound propagation may be calculated numerically. The limited number of plots shown here illustrate the way in which both the magnitude and direction of the energy flow in the sea can be controlled by the properties of the seabed, especially when these properties are such as to allow the propagation of normal modes. Of particular interest are the complex interference patterns and circulatory energy flows which this new method of presenting propagation data highlights. These preliminary intensity vector plots are considered to be of sufficient interest to justify further numerical work using more realistic models of the seabed in which, for example, shear wave motion is included. The practical value of intensity, as opposed to pressure, measurement could be investigated by means of interacting theoretical and scale model work.

E A Skelton (HSO)

REFERENCES

1. BREKHOVSKIKH L.M., Waves in Layered Media, Academic Press, 1980.

2. BREKHOVSKIKH L., LYSANOV Yu., Fundamentals of Ocean Acoustics, Springer-Verlag, 1982.

3. GABRIELSON T.B., Mathematical Foundations for Normal Mode Modelling in Waveguides, Naval Air Development Centre, Pennsylvania, Report No. NADC-81284-30, 1980.

4. JENSEN F.B., KUPERMAN W.A., Consistency Tests of Acoustic Propagation Models, Saclant Research Centre, La Spezia, Italy, Memorandum SM-157, March 1982.

5. WOOD A.B., Model Experiments on Sound Propagation in Shallow Seas, J. Acoust. Soc. Am., 31(9), pp1213-1235, September 1959.

6. PETTERSEN O., Sound Intensity Measurements for describing Acoustic Power Flow, Applied Acoustics, 14, pp387-397, 1981.

7. SPICER W.J., Acoustic Intensity Vectors from an Infinite Plate with Line Attachments, Admiralty Marine Technology Establishment, Teddington, AMTE(N)TM81086, October 1981.

8. JAMES J.H., Acoustic Intensity Vectors inside Infinite Cylindrical Elastic Shell, Admiralty Marine Technology Establishment, Teddington, AMTE(N)TM82103, December 1982.

9. FAHY F.J., Measurements with an Intensity Meter of the Acoustic Power of a Small Machine in a Room, J. Sound. Vib., 57(3), pp311-322, 1978.

10. REINHART T.E., CROCKER M.J., Source Identification on a Diesel Engine using Acoustic Intensity Measurements, Noise Control Engineering, 18(3), pp84-92, 1982.

11. SPICER W.J., Free-wave Propagation in and Sound Radiation by Layered Media with Flow, Admiralty Marine Technology Establishment, Teddington, AMTE(N)TM82102, December 1982.

12. SKELTON E.A., Sound Radiation from a Cylindrical Pipe Composed of Concentric Layers of Fluids and Elastic Solids, Admiralty Marine Technology Establishment, Teddington, AMTE(N)TM83007, January 1983.

13. SCHULTZ T.J., et al, Measurement of Acoustic Intensity in a Reactive Sound Field, J. Acoust. Soc. Am., 57(6) Part 1, pp1263-1268, 1975.

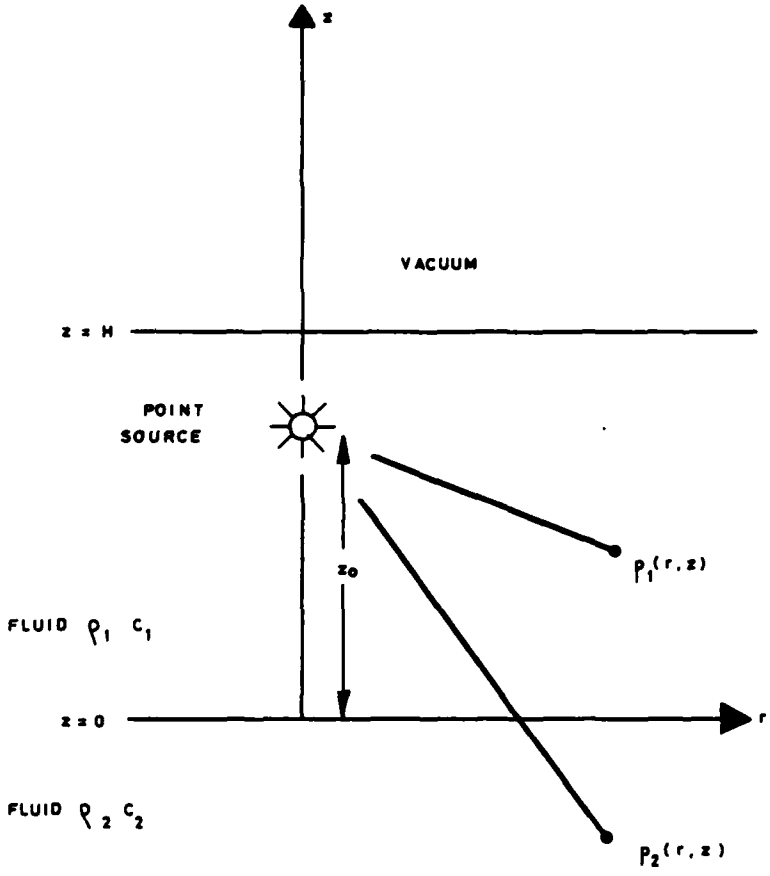

FIG. 1 GEOMETRY OF SHALLOW WATER MODEL

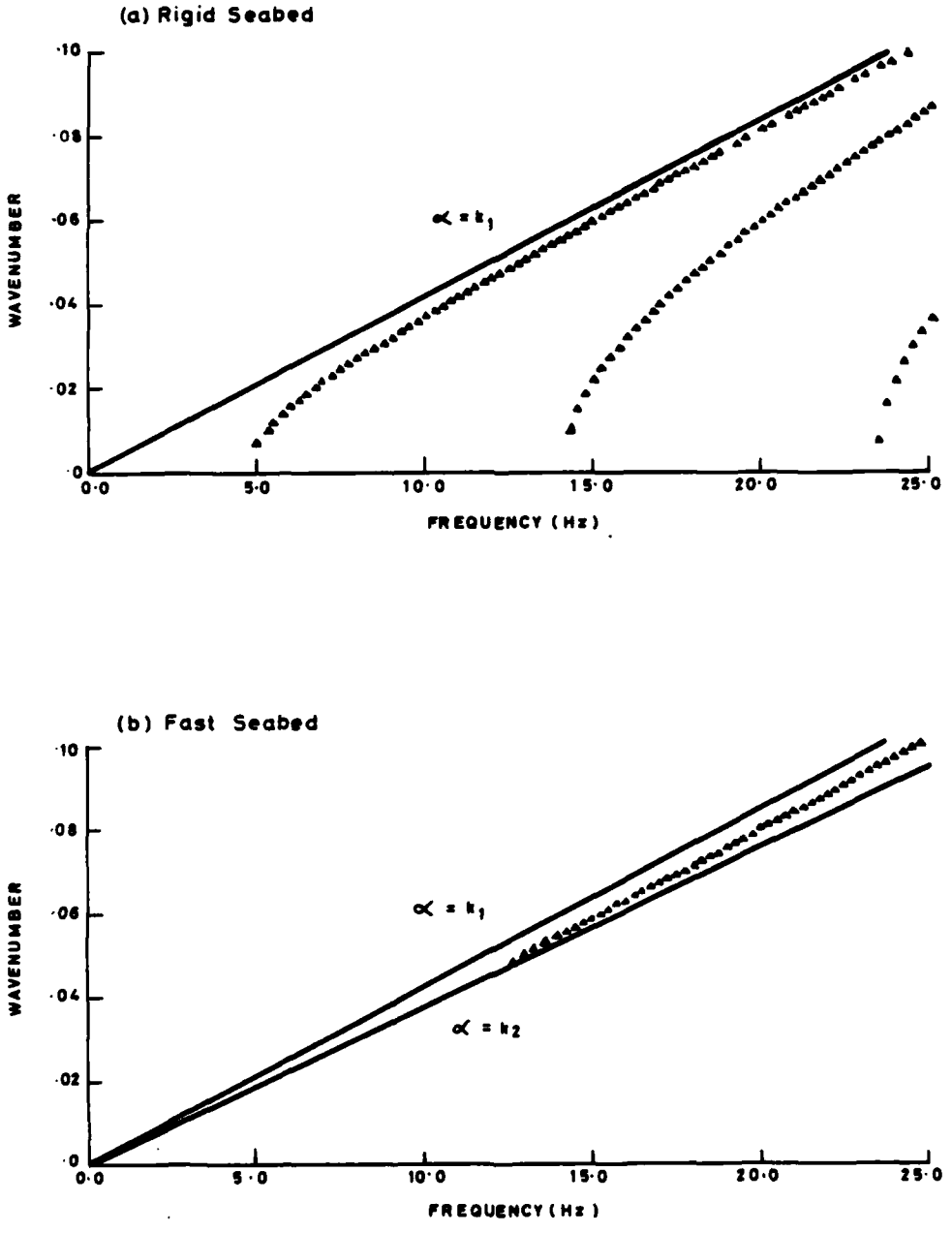

FIG. 2 RADIAL WAVENUMBER v. FREQUENCY PLOTS

(a) Slow Seabed

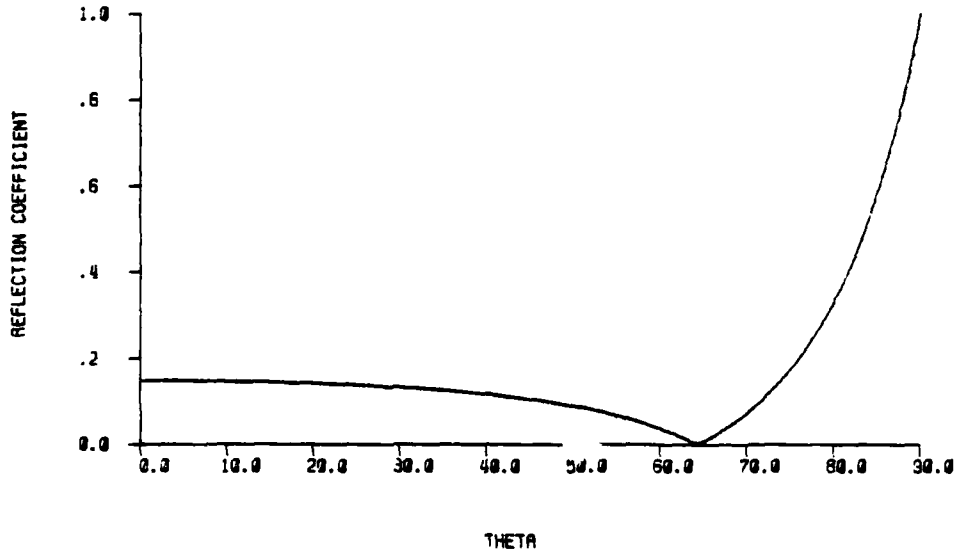

(b) Fast Seabed

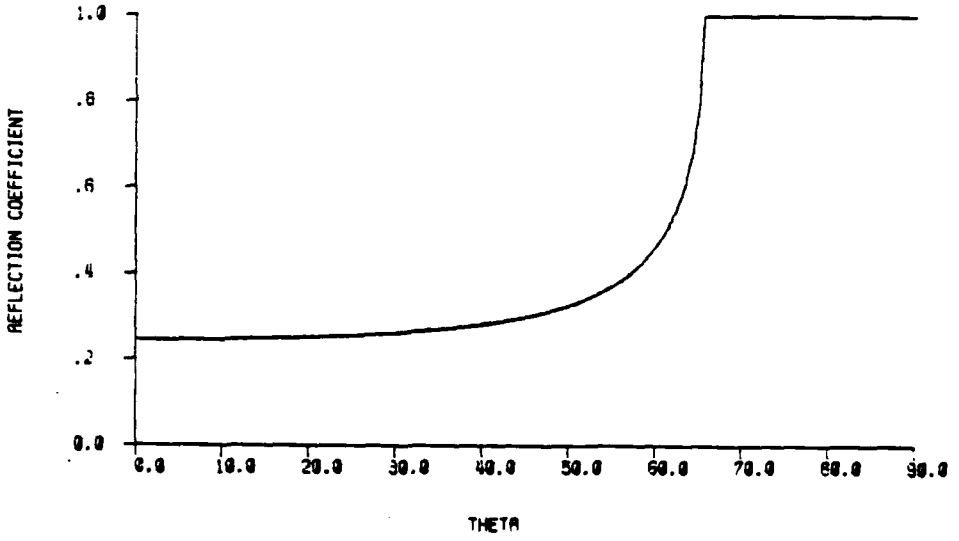

FIG. 3 REFLECTION COEFFICIENT v. ANGLE OF INCIDENCE

(a) No Seabed

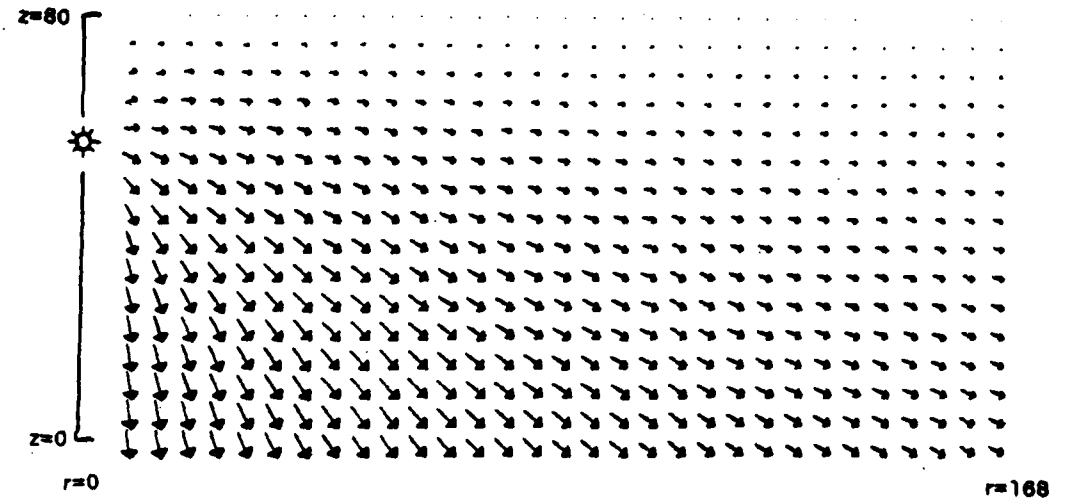

(b) Rigid Seabed

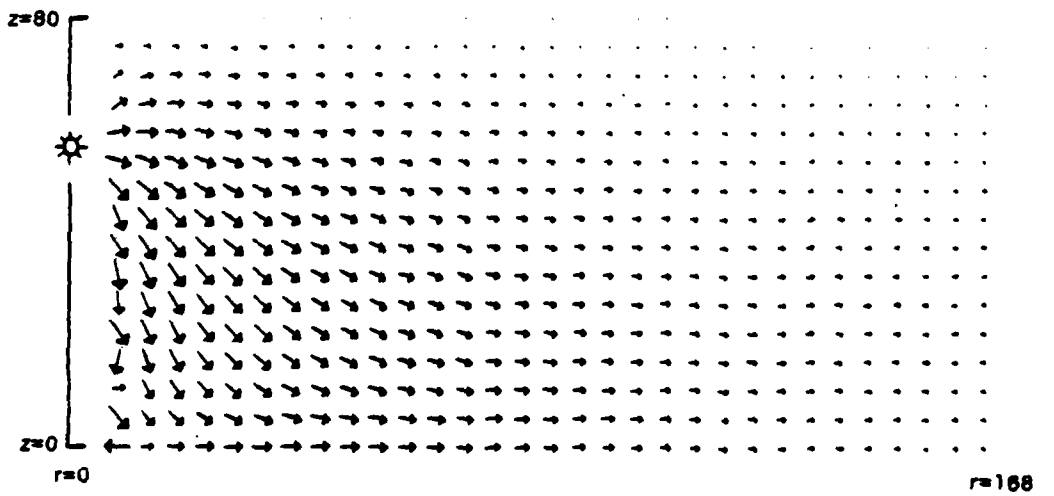

FIG. 4 INTENSITY VECTORS AT 2.5Hz

(a) Slow Seabed

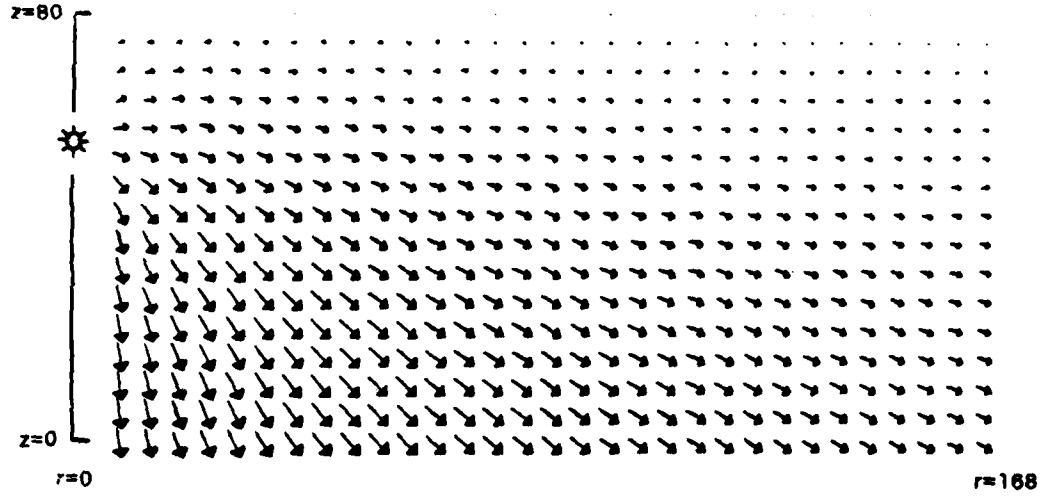

(b) Fast Seabed

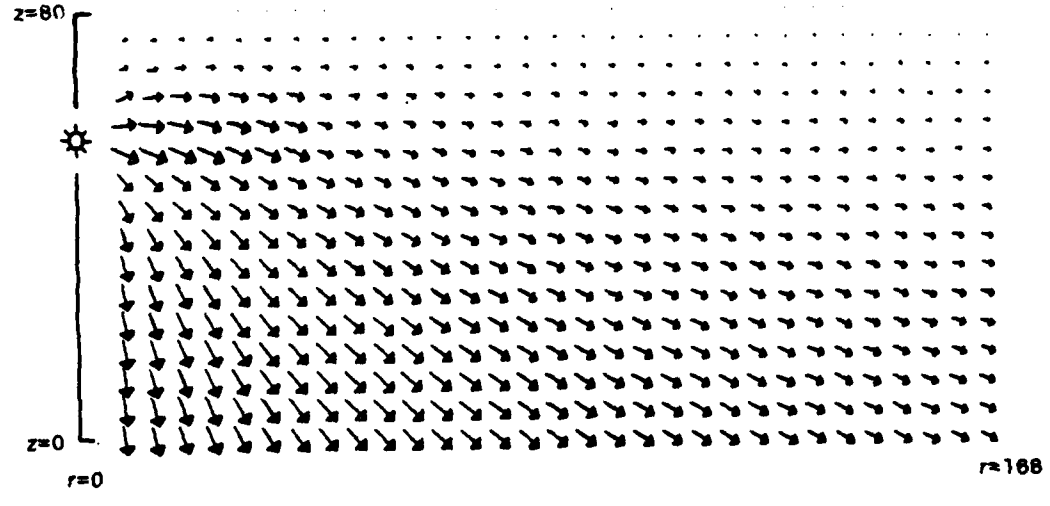

FIG. 5 INTENSITY VECTORS AT 2.5Hz

(a) No Seabed

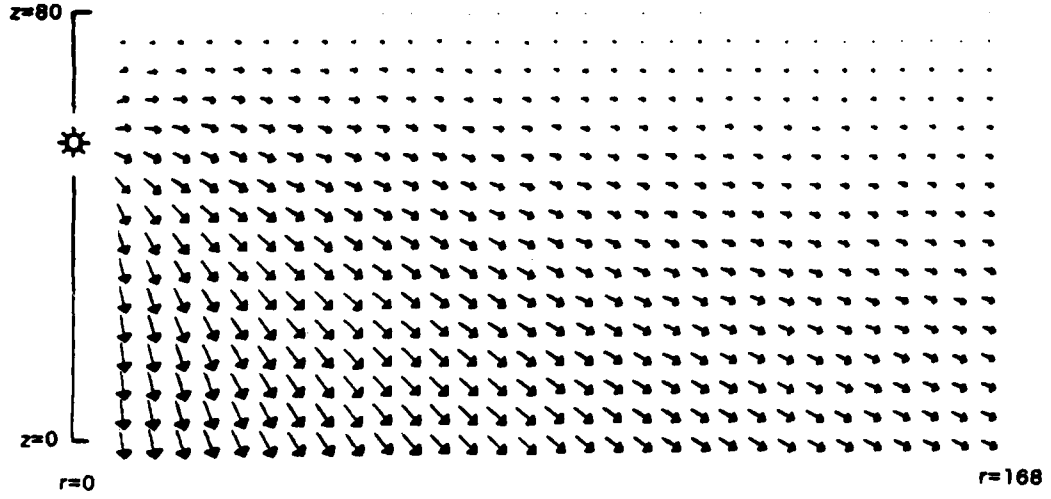

(b) Rigid Seabed

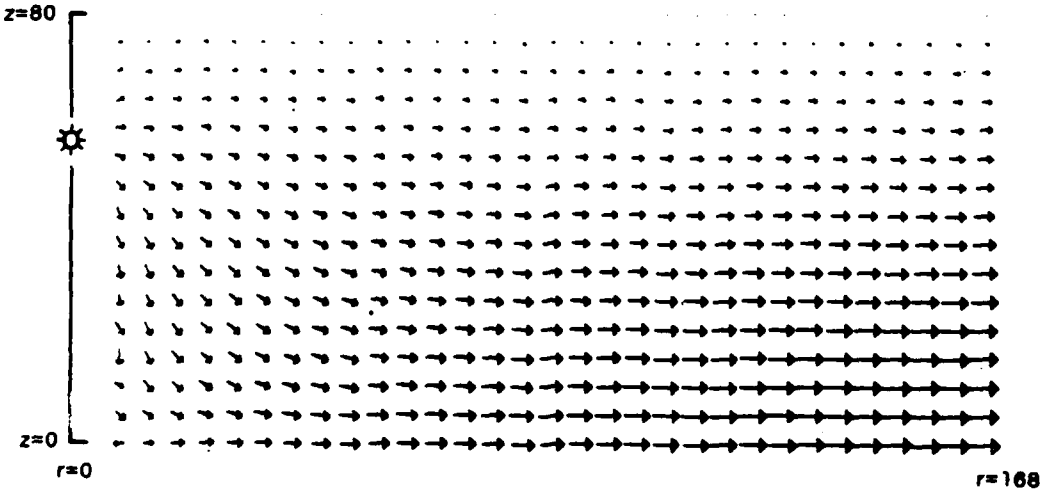

FIG. 6 INTENSITY VECTORS AT 5Hz

(a) Slow Seabed

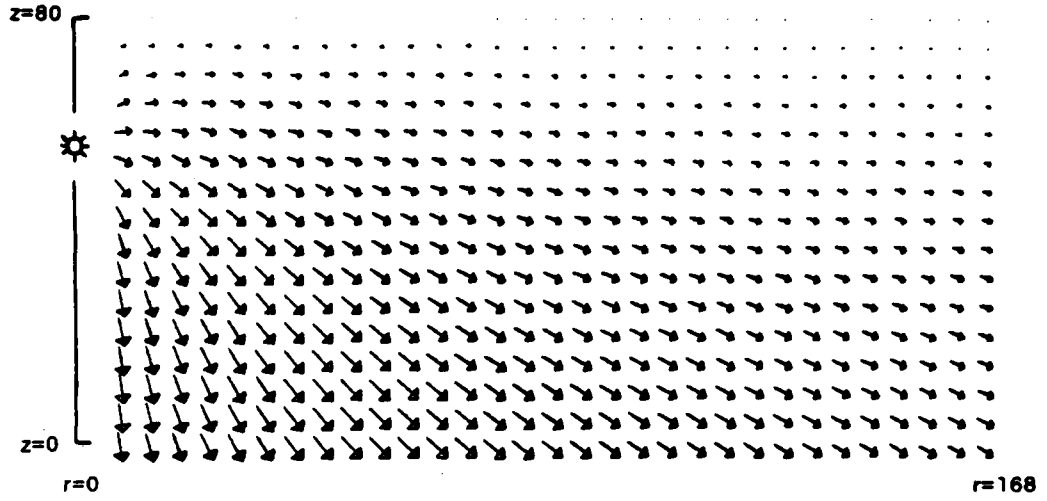

(b) Fast Seabed

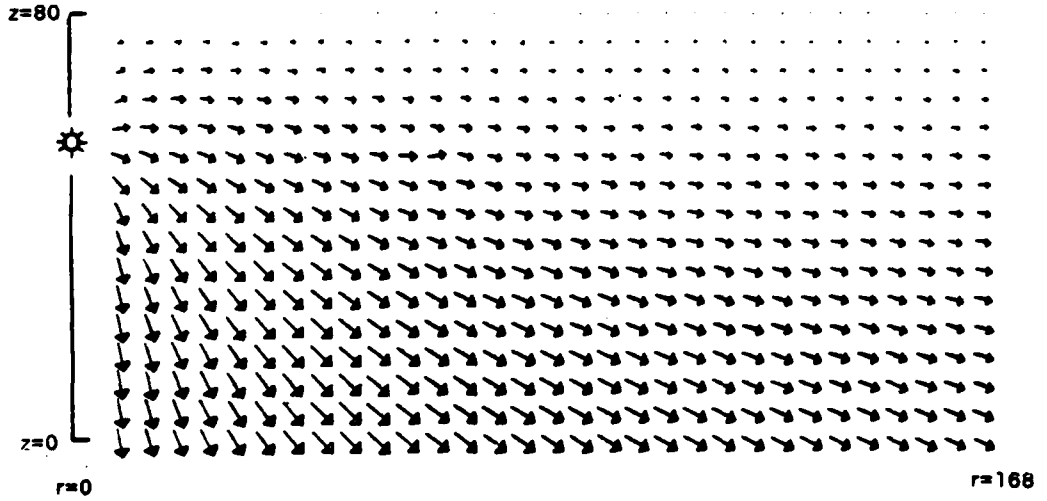

FIG. 7 INTENSITY VECTORS AT 5Hz

(a) No Seabed

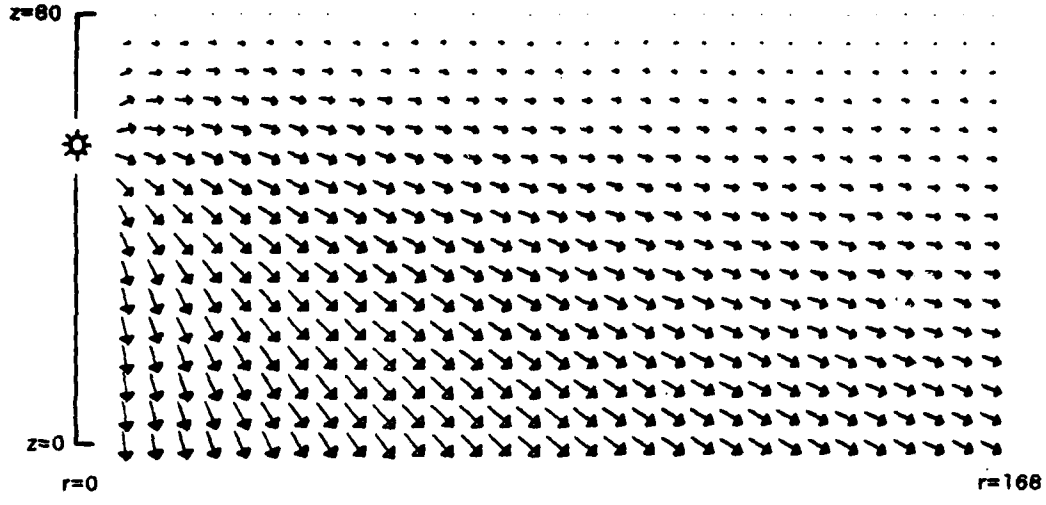

(b) Rigid Seabed

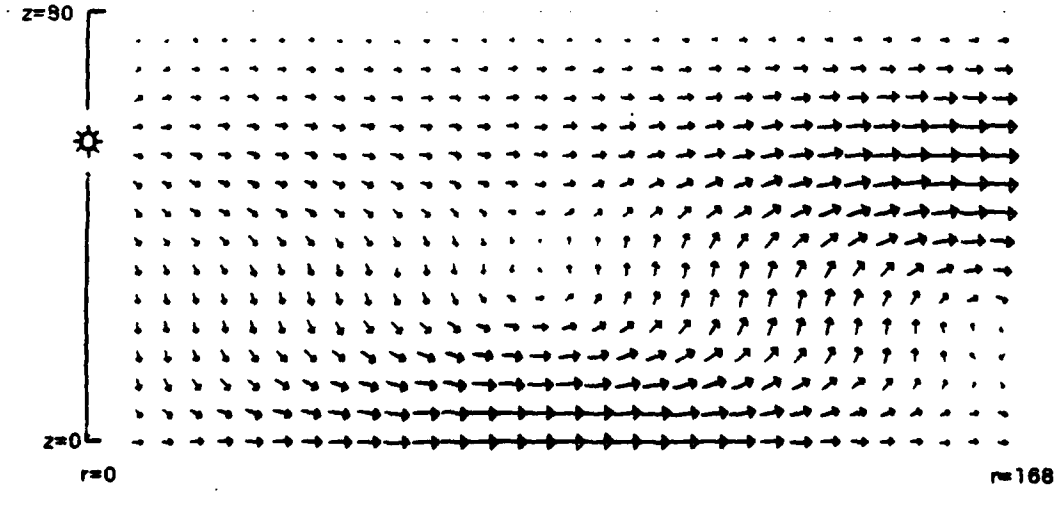

FIG. 8 INTENSITY VECTORS AT 15Hz

(a) Slow Seabed

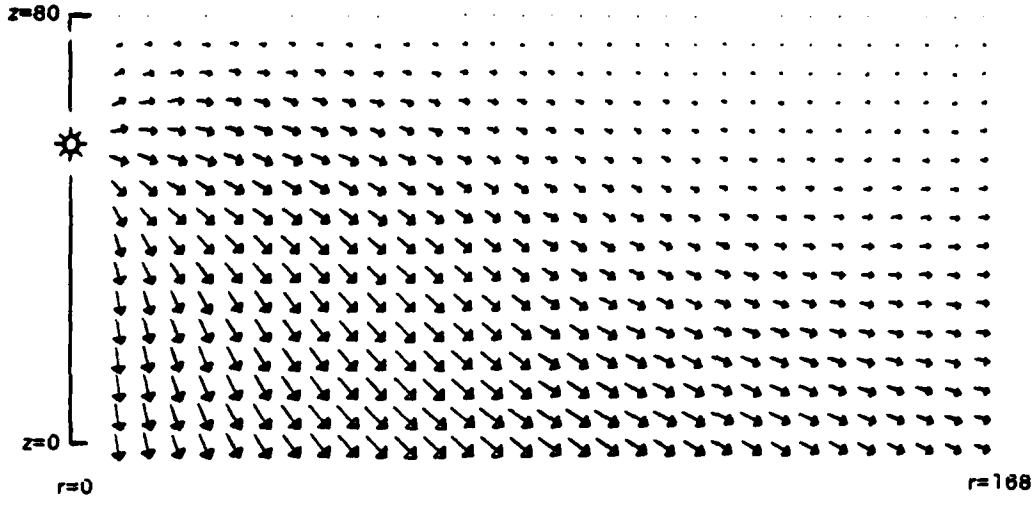

(b) Fast Seabed

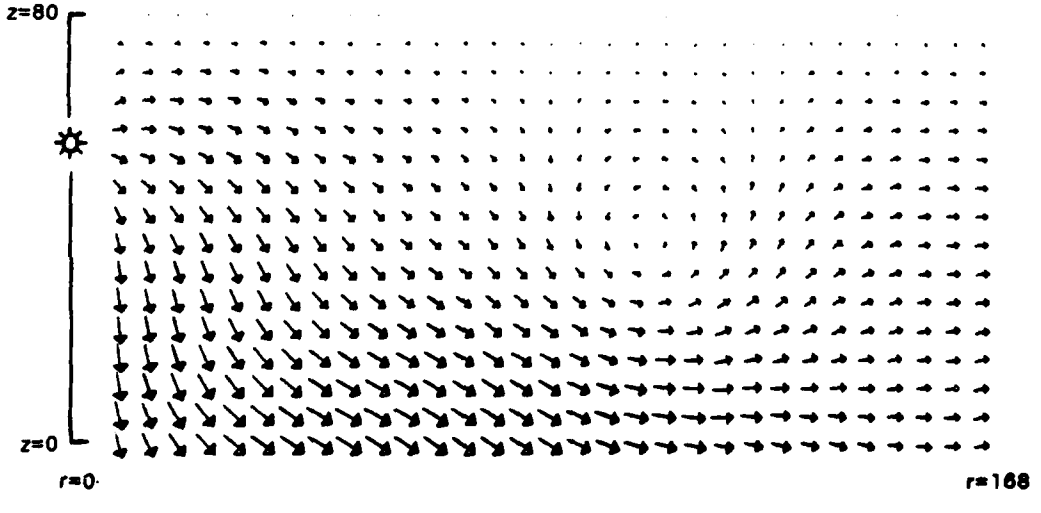

FIG. 9 INTENSITY VECTORS AT 15Hz

(a) No Seabed

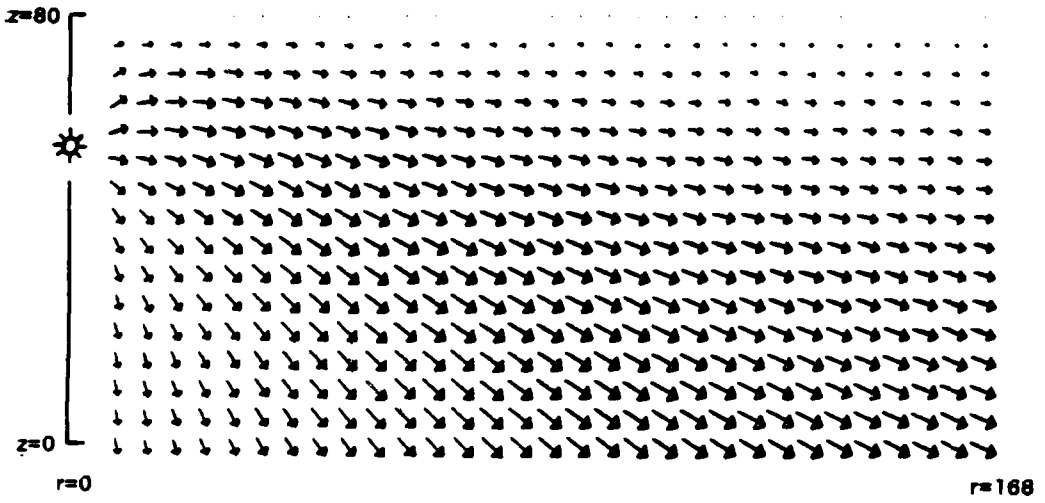

(b) Rigid Seabed

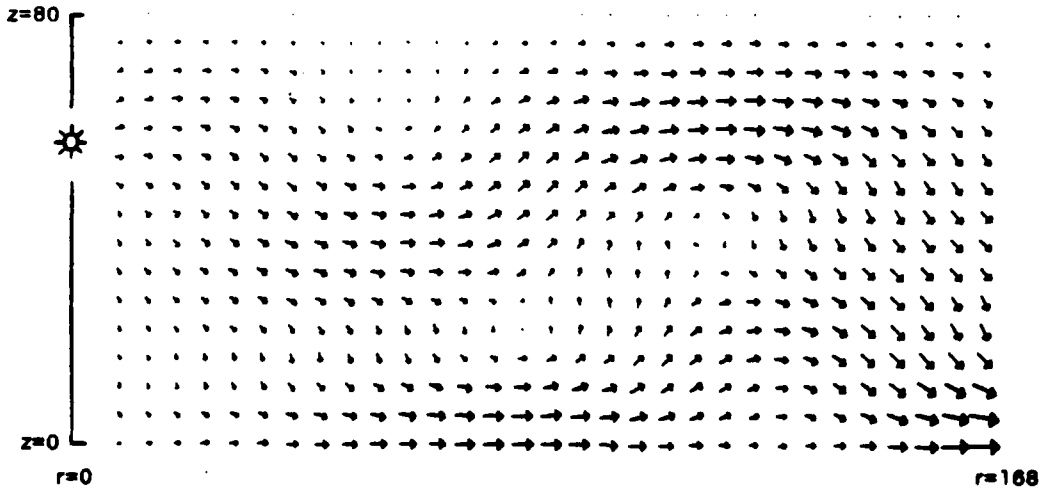

FIG. 10 INTENSITY VECTORS AT 25Hz

(a) Slow Seabed

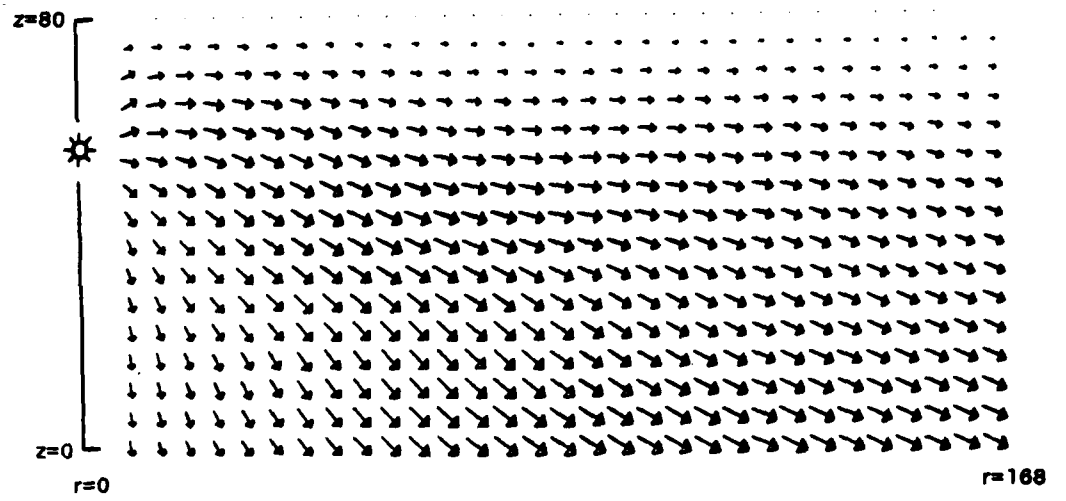

(b) Fast Seabed

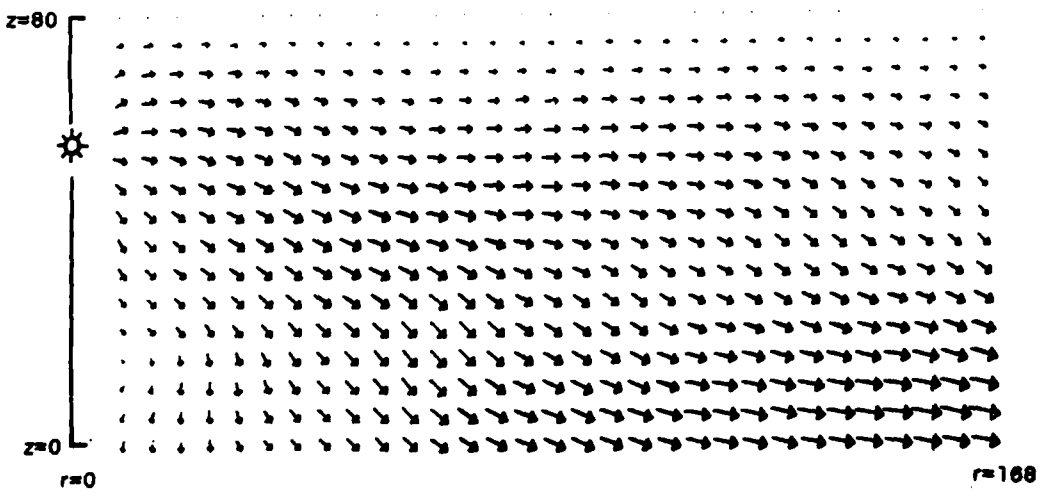

FIG. 11 INTENSITY VECTORS AT 25Hz

(a) Slow Seabed

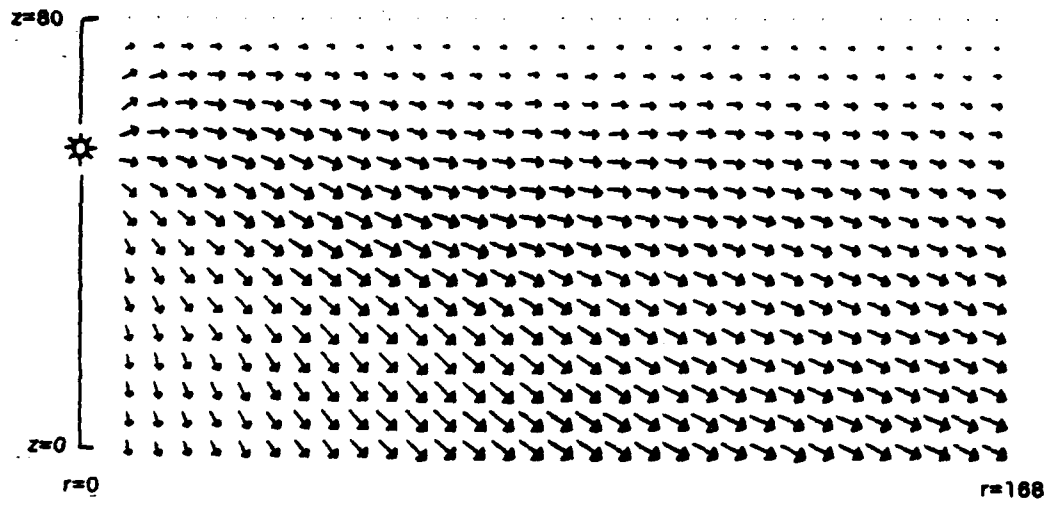

(b) Slow Seabed

Seabed Intensity

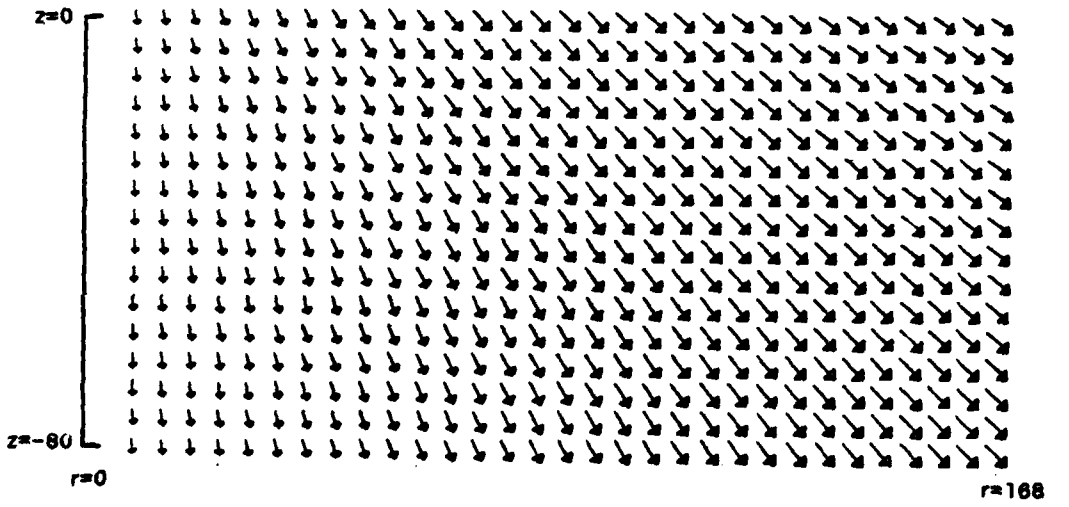

FIG. 12 INTENSITY VECTORS AT 25Hz

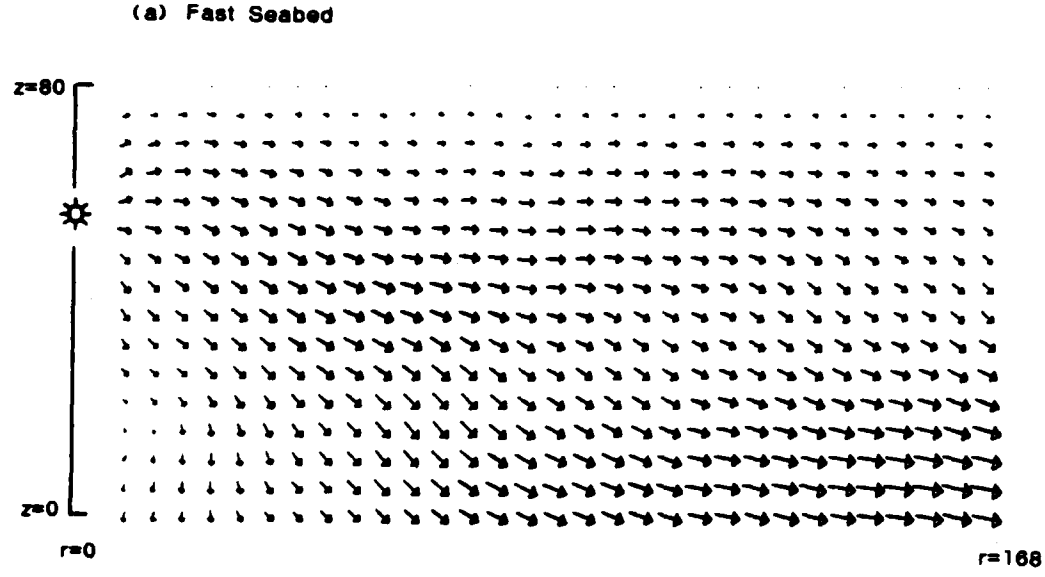

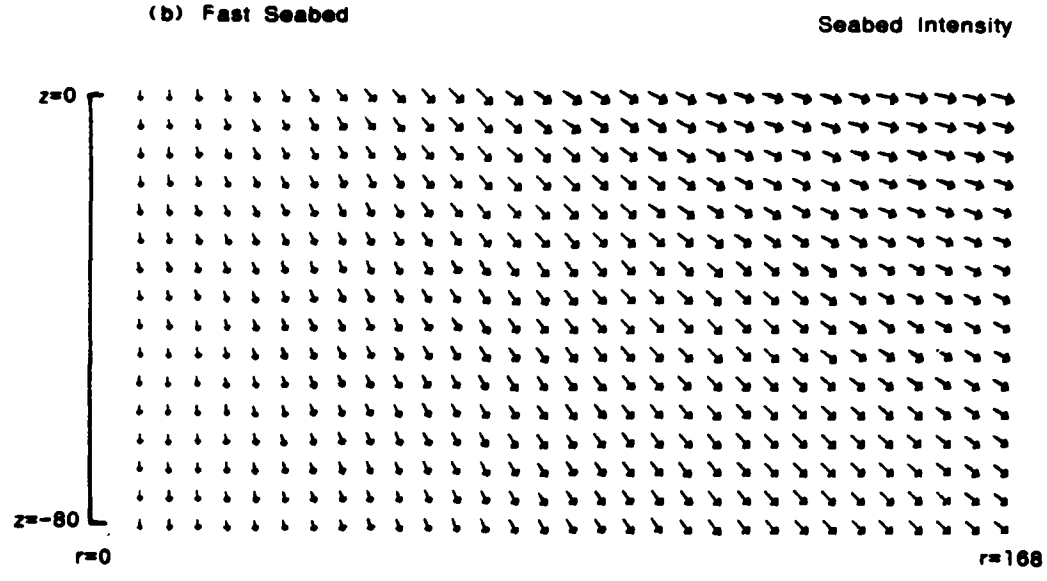

FIG. 13 INTENSITY VECTORS AT 25Hz

APPENDIX

Formulae for acoustic pressure and particle velocity of the Pekeris model

(a) No Seabed

In the special case in which the layer and the half-space consist of identical fluids, the pressure in the fluid is obtained by the method of images as

$$p_1(r,z) = p_0\exp(ik_1R_0)/R_0 - p_0\exp(ik_1R_1)/R_1 \qquad (A1)$$

where

$$R_0^2 = r^2 + (z-z_0)^2$$

$$R_1^2 = r^2 + (z+z_0-2H)^2$$

The radial and vertical particle velocities are

$$V_{1r}(r,z) = (p_0 r/i\omega\rho_1)\{(ik_1-1/R_0)\exp(ik_1R_0)/R_0^2 - (ik_1-1/R_1)\exp(ik_1R_1)/R_1^2\} \qquad (A2)$$

$$V_{1z}(r,z) = (p_0/i\omega\rho_1)\{(z-z_0)(ik_1-1/R_0)\exp(ik_1R_0)/R_0^2 - (z+z_0-2H)(ik_1-1/R_1)\exp(ik_1R_1)/R_1^2\} \qquad (A3)$$

(b) Rigid Seabed

The rigid seabed may be considered as the limiting case of the fluid half-space as $\rho_2 \to \infty$ and $c_2 \to \infty$. The well known series solution for the pressure in the fluid layer is [1]

$$p_1(r,z) = (2\pi i p_0/H)\sum_{n=0}^{\infty} \cos([2n+1]\pi z_0/2H)\cos([2n+1]\pi z/2H)H_0(\alpha_n r) \qquad (A4)$$

from which the radial and vertical particle velocities may be deduced as

$$V_{1r}(r,z)=(-2\pi p_0/\omega\rho_1 H)\sum_{n=0}^{\infty}\alpha_n\cos([2n+1]\pi z_0/2H)\cos([2n+1]\pi z/2H)H_1(\alpha_n r) \quad (A5)$$

$$V_{1z}(r,z)=(-\pi^2 p_0/\omega\rho_1 H^2)\sum_{n=0}^{\infty}(2n+1)\cos([2n+1]\pi z_0/2H)\sin([2n+1]\pi z/2H)H_0(\alpha_n r) \quad (A6)$$

(c) Fast or Slow Seabed

In the general case of the fast seabed ($c_2>c_1$) or the slow seabed ($c_2<c_1$), the pressure and particle velocities in the fluid layer are given in the region $0\le z\le z_0$ by

$$p_1(r,z)=2p_0\int_0^{\infty}\alpha\beta_1^{-1}D^{-1}J_0(\alpha r)\sin(\beta_1[H-z_0])\{\beta_1\cos(\beta_1 z)-ib\beta_2\sin(\beta_1 z)\}d\alpha \quad (A7)$$

$$V_{1r}(r,z)=(2ip_0/\omega\rho_1)\int_0^{\infty}\alpha^2\beta_1^{-1}D^{-1}J_1(\alpha r)\sin(\beta_1[H-z_0])\{\beta_1\cos(\beta_1 z)-ib\beta_2\sin(\beta_1 z)\}d\alpha \quad (A8)$$

$$V_{1z}(r,z)=(2ip_0/\omega\rho_1)\int_0^{\infty}\alpha D^{-1}J_0(\alpha r)\sin(\beta_1[H-z_0])\{\beta_1\sin(\beta_1 z)+ib\beta_2\cos(\beta_1 z)\}d\alpha \quad (A9)$$

where the dispersion relation D is

$$D(\alpha,\omega)=\beta_1\cos(\beta_1 H)-ib\beta_2\sin(\beta_1 H)$$

and in the region $z_0\le z\le H$ by

$$p_1(r,z)=2p_0\int_0^{\infty}\alpha\beta_1^{-1}D^{-1}J_0(\alpha r)\sin(\beta_1[H-z])\{\beta_1\cos(\beta_1 z_0)-ib\beta_2\sin(\beta_1 z_0)\}d\alpha \quad (A10)$$

$$V_{1r}(r,z)=(2ip_0/\omega\rho_1)\int_0^{\infty}\alpha^2\beta_1^{-1}D^{-1}J_1(\alpha r)\sin(\beta_1[H-z])\{\beta_1\cos(\beta_1 z_0)-ib\beta_2\sin(\beta_1 z_0)\}d\alpha \quad (A11)$$

$$V_{1z}(r,z)=(2ip_0/\omega\rho_1)\int_0^\infty \alpha D^{-1}J_0(\alpha r)\cos(\beta_1[H-z])(\beta_1\cos(\beta_1 z_0)-ib\beta_2\sin(\beta_1 z_0))d\alpha \tag{A12}$$

The pressure and particle velocities in the lower half-space are

$$p_2(r,z) = 2p_0\int_0^\infty \alpha D^{-1}J_0(\alpha r)\sin(\beta_1[H-z_0])\exp(-i\beta_2 z)d\alpha \tag{A13}$$

$$V_{2r}(r,z)=(2ip_0/\omega\rho_2)\int_0^\infty \alpha^2 D^{-1}J_1(\alpha r)\sin(\beta_1[H-z_0])\exp(-i\beta_2 z)d\alpha \tag{A14}$$

$$V_{2z}(r,z) = (-2p_0/\omega\rho_2)\int_0^\infty \alpha\beta_2 D^{-1}J_0(\alpha r)\sin(\beta_1[H-z_0])\exp(-i\beta_2 z)d\alpha \tag{A15}$$

END

DATE
FILMED

10 83

DT